Non-coding RNA Research 10 (2025) 116–129

Contents lists available at ScienceDirect

Non-coding RNA Research

journal homepage: www.keaipublishing.com/en/journals/non-coding-rna-research

Original Research Article

ADAR1-regulated miR-142-3p/RIG-I axis suppresses antitumor immunity in nasopharyngeal carcinoma

Haoyuan Xu [a,1], Wanpeng Li [a,1], Kai Xue [a,1], Huankang Zhang [a], Han Li [a], Haoran Yu [b], Li Hu [a], Yurong Gu [a], Houyong Li [a], Xicai Sun [a,**], Quan Liu [a,***], Dehui Wang [a,*]

[a] Department of Otolaryngology-Head and Neck Surgery, Affiliated Eye Ear Nose and Throat Hospital, Fudan University, Shanghai, 200031, China
[b] Department of Otorhinolaryngology-Head and Neck Surgery, Affiliated Zhongshan Hospital, Fudan University, Shanghai, 200030, China

ARTICLE INFO

Keywords:
Nasopharyngeal carcinoma
miR-142-3p
RIG-I
Tumor immune response

ABSTRACT

Following the initial treatment of nasopharyngeal carcinoma (NPC), tumor progression often portends an adverse prognosis for these patients. MicroRNAs (miRNAs) have emerged as critical regulators of tumor immunity, yet their intricate mechanisms in NPC remain elusive. Through comprehensive miRNA sequencing, tumor tissue microarrays and tissue samples analysis, we identified miR-142-3p as a significantly upregulated miRNA that is strongly associated with poor prognosis in recurrent NPC patients. To elucidate the underlying molecular mechanism, we employed RNA sequencing, coupled with cellular and tissue assays, to identify the downstream targets and associated signaling pathways of miR-142-3p. Our findings revealed two potential targets, CFL2 and WASL, which are directly targeted by miR-142-3p. Functionally, overexpressing CFL2 or WASL significantly reversed the malignant phenotypes induced by miR-142-3p both in vitro and in vivo. Furthermore, signaling pathway analysis revealed that miR-142-3p repressed the RIG-I-mediated immune defense response in NPC by inhibiting the nuclear translocation of IRF3, IRF7 and p65. Moreover, we discovered that ADAR1 physically interacted with Dicer and promoted the formation of mature miR-142-3p in a dose-dependent manner. Collectively, ADAR1-mediated miR-142-3p processing promotes tumor progression and suppresses antitumor immunity, indicating that miR-142-3p may serve as a promising prognostic biomarker and therapeutic target for NPC patients.

1. Introduction

Nasopharyngeal carcinoma (NPC), an epithelial malignancy originating from the mucosal lining of nasopharynx, exhibits a distinct geographical distribution, predominantly affecting individuals in South and East Asia, North America, and Northern Europe. According to GLOBOCAN data, these regions have age-standardized rates ranging from 4 to 25 cases per 100,000 individuals [1–3]. Recently, immunotherapy, particularly immune checkpoint inhibitors (ICIs), has offered therapeutic hope to numerous patients with advanced NPC [4]. However, a substantial proportion of NPC patients fail to respond to immunotherapy, emphasizing the need to investigate the molecular and signaling pathways contributing to NPC immunotherapy resistance and identify potential targets for sensitization.

MicroRNAs (miRNAs), highly conserved noncoding RNAs of approximately 22 nucleotides, functions as regulators of gene expression by binding to sequences in the coding DNA sequence (CDS) or 3′ untranslated regions (3′-UTRs) of target mRNAs, ultimately leading to their degradation [5,6]. Numerous studies have underscored the crucial role of miRNAs in modulating malignant phenotypes [7–9], positioning them as promising candidates for effective biomarkers and therapeutic targets [10]. Moreover, miRNAs are intricately associated with antitumor immunity. For instance, EBV-miR-BART11 and EBV-miR-BART17-3p

* Corresponding author. Department of Otolaryngology-Head and Neck Surgery, Affiliated Eye Ear Nose and Throat Hospital, Fudan University, 83 Fen Yang Road, Shanghai, China.
** Corresponding author. Department of Otolaryngology-Head and Neck Surgery, Affiliated Eye Ear Nose and Throat Hospital, Fudan University, 83 Fen Yang Road, Shanghai, China.
*** Corresponding author. Department of Otolaryngology-Head and Neck Surgery, Affiliated Eye Ear Nose and Throat Hospital, Fudan University, 83 Fen Yang Road, Shanghai, China.
E-mail addresses: laryngeal@163.com (X. Sun), liuqent@163.com (Q. Liu), wangdehuient@sina.com (D. Wang).
[1] Haoyuan Xu, Wanpeng Li, and Kai Xue contributed equally to this article.

https://doi.org/10.1016/j.ncrna.2024.08.003
Received 24 June 2024; Received in revised form 4 August 2024; Accepted 14 August 2024
Available online 15 August 2024

List of abbreviations

NPC	Nasopharyngeal carcinoma
MiRNAs	MicroRNAs
Co-IP	Co-immunoprecipitation
EMSA	Electrophoretic mobility shift assays
ADAR1	Adenosine deaminases acting on RNA1
CFL2	Cofilin 2
WASL:	Wiskott-Aldrich syndrome like
RIG-I:	Retinoic acid-inducible gene I
ICIs	Immune checkpoint inhibitors
CDS	Coding DNA sequence
UTR	Untranslated region
EBV	Epstein−Barr virus
MAVS	Mitochondrial antiviral signaling
FBS	Fetal bovine serum
KD	Knockdown
OE	Overexpression
RT-PCR :	Real-time polymerase chain reaction
GAPDH	Glyceraldehyde phosphate dehydrogenase gene
TBST	Tris buffered saline Tween
CCK-8	Cell counting kit-8
FITC	Fluorescein isothiocyanate
FISH	Fluorescence in situ hybridization
DAPI	4′,6-diamidino-2-phenylindole
IHC	Immunohistochemistry
LC-MS	Liquid chromatography mass spectrometry
ELISA	Enzyme-linked immunosorbent assay
RIP	RNA immunoprecipitation
IF	Immunofluorescence
PBS	Phosphate buffered saline
ELISA	Enzyme-linked immunosorbent assay
TCGA	The Cancer Genome Atlas
OS	Overall survival
PFS	Progression-free survival
MFS	Metastasis-free survival
DSBs	Double-strand DNA breaks
IFN	Type I interferon
GOBP	Gene Ontology biological processes
GSEA	Gene set enrichment analysis
NSCLC	Non-small cell lung cancer
HMGB1	High mobility group box-1
PD-L1	Programmed death ligand-1
RLRs	RIG-I–like receptors

inhibit FOXP1 and PBRM1, respectively, while enhanceing the PD-L1 transcription, thus promoting EBV-associated tumor immune escape [11]. In liver cancer, miR-22 promotes antitumor immunity by reducing the abundance of IL-17-producing T cells and inhibiting IL-17 signaling [12]. Elucidating the novel mechanisms of miRNAs involved in tumor immunity could provide a theoretical foundation for discovering novel therapeutic targets.

Growing evidence underscores the multifaceted role of ADARs in diverse biological processes via RNA editing-independent mechanisms, including gene expression regulation [13], miRNA generation [14,15] and protein−protein complex formation [16]. Recent investigations have highlighted a robust interaction between Dicer and ADAR1, where ADAR1 augments the rate of miRNA processing by Dicer [17,18]. In E11–12 embryos, elevated expression of Dicer and ADAR1 p100 enhanced the capacity for pri-miRNA processing [14]. As a result of RNA editing, inosines are interpreted as guanosines by the cellular machinery and are base-paired with cytosine, analogous to an A to I substitution [19]. Accordingly, editing of coding mRNAs may introduce stop codons, modify splice sites, or induce missense codons, leading to recoding and yielding structurally and functionally unique isoforms of proteins from the same transcript. Intriguingly, editing a primary miRNA often affects its biogenesis and thus inhibits miRNA maturation. Therefore, this intricate and underexplored mechanism highlights the complex effects of ADAR1 on miRNAs in specific contexts.

In this study, we performed a comparative analysis of differentially expressed miRNAs in matched primary and recurrent NPC tissues using miRNA sequencing. The results revealed that miR-142-3p was overexpressed in recurrent NPC (rNPC) and was associated with adverse prognosis. Further transcript sequencing results demonstrated that miR-142-3p directly binds to CFL2 and WASL, promoting tumor progression and suppressing antitumor immunity by impeding the RIG-I-MAVS pathway. Remarkably, we also proved that ADAR1 could physically interact with Dicer and facilitate the biogenesis of miR-142-3p in an A to I editing-independent manner.

2. Materials and methods

2.1. Clinical samples and microarray assay

To validate the expression levels of miR-142-3p, CFL2 and WASL in NPC tissue samples, we collected recurrent and primary tumor tissue samples from patients diagnosed with NPC through pathological examination at the Department of Otorhinolaryngology of the Affiliated Eye, Ear, Nose, and Throat Hospital (AEENTH), Fudan University (Shanghai, China). The NPC microarray was purchased from Tufeibio (Shanghai, China), which encompassed 122 tissue spots derived from NPC patients, enabling a comprehensive clinical evaluation. Clinical data, such as sex, age, stage, distant metastasis, cervical lymph node metastasis, and time from initial treatment to recurrence or metastasis event, were recorded for these cases. The clinical stages of all enrolled NPC patients adhered to the 8th edition of the American Joint Committee on Cancer Staging Manual. The Kaplan–Meier method was employed to construct survival curves for overall, progression-free and metastasis-free survival based on the relative expression levels of miR-142-3p. All patients offered their tissue samples voluntarily, and we obtained their verbal informed consent. The study was approved by the Institutional Review Board of AEENTH, Fudan University.

2.2. Cell culture

All of human nasopharyngeal cancer-derived cell lines used in this study were obtained from the Xiangya Hospital Affiliated to Central South University (Hunan, China). These cells were cultured in RPMI 1640 (HyClone, USA) supplemented with 10 % foetal bovine serum (FBS, Thermo Fisher Scientific) and 1 × antibiotic/antimycotic solution (Corning, USA). Cells were maintained at 37 °C in a 5 % CO_2 incubator, prepared for subsequent experiments.

2.3. miRNA sequencing and mRNA sequencing

For miRNA sequencing, total RNA was extracted from primary and recurrent tumor tissues using the mirVana miRNA Isolation Kit (Ambion) according to the manufacturer's protocol. Quantitation of the extracted total RNA was carried out using the Nanodrop 2000 (Thermo Fisher Scientific Inc., USA). RNA integrity was assessed by Agilent 2100 Bioanalyzer (Agilent Technology, USA). 1 μg total RNA of each sample was used for the small RNA library construction using NEBNext Small RNA Library Prep Set for Illumina kit (Cat. No. NEB#E7330S, NEB, USA) following the manufacturer's recommendations. Briefly, total RNA were ligated to adapters at each end. Then the adapter-ligated RNA were

reverse transcribed to cDNA and performed PCR amplification. The PCR products ranging from 140 to 160 bp were isolated and purified as small RNA libraries. Library quality was assessed on the Agilent Bioanalyzer 2100 system. The libraries were finally sequenced using the Illumina Novaseq 6000 platform. 150 bp paired-end reads were generated.

For mRNA sequencing, total RNA was extracted the cells from the miR-142-3p overexpression group and the control group using the TRIzol reagent (Invitrogen, CA, USA) according to the manufacturer's protocol. RNA purity and quantification were evaluated using the NanoDrop 2000 spectrophotometer (Thermo Scientific, USA). RNA integrity was assessed using the Agilent 2100 Bioanalyzer (Agilent Technologies, Santa Clara, CA, USA). Then the libraries were constructed using VAHTS Universal V6 RNA-seq Library Prep Kit according to the manufacturer's instructions. Both miRNA sequencing and mRNA sequencing, as well as their subsequent analyses, were conducted by OE Biotech Co., Ltd. (Shanghai, China).

2.4. Transient transfection

The plasmids encoding RIG-I and ADAR1, along with their respective siRNAs (siRIG-I and siADAR1), miR-142-3p mimics, miR-142-3p inhibitors, and their respective negative controls, were obtained from Genomeditech (Shanghai, China). The NPC cell lines, 5–8F and CNE-2, were seeded in 6-well plates at a density of 2×10^5 cell per well and incubated overnight. Subsequently, two 1.5 ml EP tubes, labeled as tube A and tube B, were prepared. Each tube was supplemented with 250 μl Opti-MEM I (Thermo Fisher, CA, USA). Then, 10 μl lipofectamine 2000 (Thermo Fisher, CA, USA) was added to tube A, whereas the corresponding plasmids (4 μg), or siRNAs (10 μl), or mimics (10 μl), or inhibitors (10 μl) was added to tube B. Both tubes were left undisturbed for 5min. Then tube A was gently mixed into tube B and allowed to stand for an additional 20min to ensure complete complexation. Afterward, this complex mixture was diluted in 1.5 ml of serum-free medium, thoroughly mixed, and subsequently added to the 2 ml of 6-well plates already containing the NPC cells. After 6-h incubation period, the medium was replaced with fresh RPMI-1640 supplemented with 10 % FBS and the cells were further incubated in a humidified environment at 37 °C with 5 % CO_2 for 48h.

2.5. Establishment of stable NPC cell lines

The shRNA plasmids targeting miR-142-3p, CFL2 or WASL were used for their knockdown and the target sequences for the human miR-142-3p shRNA was 5′-TCCATAAAGTATTCACACTACA-3′, for the human CFL2 shRNA was 5′-CCTCTGAATGATTGCCGATAT-3′, and for the human WASL shRNA was 5′-GCACAACTTAAAGACAGAGAA-3'. The lentivirus plasmids containing miR-142-3p, CFL2 or WASL was used for thier overexpression. The plasmids stably expressing miR-142-3p, CFL2 and WASL, as well as the knockdown plasmids, were devised and purchased from Genomeditech (Shanghai, China). The indicated cells were seeded into a 6-well plate and cultured in a 37 °C incubator with 5 % CO_2 until they reached about 60 % confluence. 50 μl of the lentivirus suspension and Polybrene (Genomeditech, Shanghai, China) at a final concentration of 6 μg/ml were added to each well. The mixture was incubated in 5 % CO_2 at 37 °C for 24h. Following this infection period, the lentiviral-containing medium was replaced with fresh culture medium. The cells were then further incubated at 37 °C for an additional 48h. Subsequently, puromycin (Thermo Fisher, CA, USA) was introduced to the culture at a final concentration of 1 μg/ml to select for cells that had successfully integrated the lentiviral vector. After two-week selection process, cell samples were harvested, and the transfection efficiency was detected through RT-PCR analysis.

2.6. RNA extraction and RT-PCR analysis

Total RNA was isolated from the indicated tissues or cells using Trizol reagent (Invitrogen, USA). The tissue samples were pre-separated and processed using an ultrasound apparatus. The samples were mixed with 1 ml Trizol and transferred to a 1.5 ml EP tube. 200ul of chloromethane was added, and the samples were shaken vigorously and centrifuged at 4 °C for 15min at 12,000 rpm to separate the RNA, DNA and protein layers. The upper aqueous phase was carefully extracted into a new enzyme-free EP tube. After adding 500ul precooled isopropanol, the mixture was gently reversed and mixed, and the mixture was allowed to stand at room temperature for 10min. After further centrifugation at 4 °C for 10min at 12,000 rpm, the supernatant was discarded, and the RNA precipitate was washed with 1 ml of 75 % alcohol. After centrifugation at 4 °C for 5min at 7500 rpm, the supernatant was discarded. The RNA residue was dissolved in 50ul Diethylpyrocarbonate (DEPC) treated water. The RNA concentration was determined using a Nanodrop spectrophotometer. The isolated RNA underwent reverse transcription into cDNA using the Evo M-MLV RT premix (Agbiotech, USA) in a single-step reaction.Regardless of the extracted RNA concentration, each sample's total volume was less than 10 μl. A 0.2 ml centrifuge tube was filled with 1 μg RNA, 2 μl of 5 × reaction buffer, and the remaining nuclease-free water. The tubes were incubated at 37 °C for 15min, followed by 85 °C for 5sec, and then maintained at 4 °C. The reaction's products were chilled on ice and briefly centrifuged. RT-PCR was performed using the SYBR Green Premix Pro Taq HS qPCR kit (Agbiotech) on a 7500 Real-Time PCR System (Applied Biosystems, Carlsbad, CA, USA). U6 RNA and GAPDH were used as the internal controls. Each tube contained 1 μl of cDNA, 3 μl of RNAse-free water, 5 μl 2 × SYBR Green Pro Taq HS Premix II, 0.5 μl forward primer, and 0.5 μl reverse primer, The RT-PCR cycling conditions were 10min at 95 °C, 40 cycles for 5sec at 95 °C, and a 60°C-annealing temperature for 1min. The relative expression levels were evaluated using the $2-\Delta\Delta Ct$ method. The sequences of primers used in this study were shown in Table S1.

2.7. Western blot analysis

Standard protocols were followed for Western blot analysis. Indicated cells cultured in 6-well plates were harvested during the logarithmic growth phase and subjected to two rounds of washing with PBS. Subsequently, 200 μl RIPA lysis buffer (Beyotime, Shanghai, China) combined with 1 mM of protease inhibitor (or phosphatase inhibitor) (Beyotime, Shanghai, China) was employed to extract total protein. In addition, Nuclear and Cytoplasmic Protein Extraction Kit (Beyotime, Shanghai, China) was used to separate and extract the protein in nucleus and cytoplasm. Adherent cells were scraped off and immediately resuspended in 200 μl cytosolic protein extraction reagent A supplemented with PMSF. The suspension was vortexed for 5sec, followed by incubation for 10min. Subsequently, 10 μl cytosolic protein extraction reagent B was added, followed by another 5-s vortexing and 1-min incubation. The mixtuer was then centrifugated at 12,000 rpm for 15min at 4 °C. The resulting supernatant, containing the cytosolic proteins, was aspirated into a precooled 1.5 ml EP tube. For nuclear protein extraction, the remaining precipitate was subjected to complete aspiration of the supernatant, followed by the addition of 50 μl nuclear protein extraction reagent supplemented with PMSF. The cells were vortexed for 15sec and then placed in an ice bath, with additional vortexing for 15sec every 2min for a total of 30min. Following centrifugation at 12,000 rpm for 10min at 4 °C, the supernatant was transferred to a pre-cooled plastic tube. Protein concentrations were determined using a BCA assay kit (Thermo Fisher Scientific Inc., USA). For protein separation, 20 μg of protein samples was loaded onto an SDS-PAGE gel, and the resolved proteins were then electrotransferred onto a PVDF membrane. The membrane was blocked with TBST buffer containing 5 % skimmed milk for 1h at room temperature. After blocking, the membrane was incubated overnight at 4 °C with primary antibodies. The membrane underwent washing with TBST three times. Folloing this, the membrane was incubated with appropriate secondary antibodies for 1.5h at room

temperature. Post-incubation, the membrane was again subjected to three washes with TBST, and an ECL reagent was applied to induce luminescence. Bands were detected by a Bio-Rad ChemiDoc XRS system. The antibodies used in this study were listed in Table S2.

2.8. CCK-8 assay, clonogenic survival assay and apoptosis assay

To evaluate cell proliferation, 1000 transfected 5–8F cells and CNE-2 cells were seeded in 100 μl of complete culture media per well in 96-well plates and cultured for indicated time periods. After 24, 48, 72, 96, and 120h, 10 μl CCK-8 (Dojindo Laboratories, Kumamoto, Japan) reagent was added into each well, followed by incubation for 2h at 37 °C. Then, cell viability was determined by scanning with a microplate reader at 450 nm. For the colony formation assay, 500 transfected 5–8F cells and CNE-2 cells were plated in 1 ml of complete culture media per well in 12-well plates and incubated for 7 days. After 7 days, colonies were stained with crystal violet and quantified using ImageJ software. For apoptosis analysis, 5×10^5 transfected 5–8F cells and CNE-2 cells were harvested by centrifugation and resuspended in 100 μl 1 × Binding Buffer within 1.5 ml EP tubes. The cells were then stained with 5 μl Annexin V conjugated with fluorescein isothiocyanate (FITC) and 5 μl propidium iodide (PI). Following gently vortexing, the cells were incubated in the dark at room temperature for 15min. 400 μl of 1 × Binding Buffer was added to each tube, and cells were analyzed using a FACSCalibur System immediately. The relative percentage of Annexin V–positive cells was determined using CellQuest Pro software. All assays were performed in triplicate three times.

2.9. Immunofluorescence (IF) assay

Briefly, exponentially growing transfected 5–8F cells and CNE-2 cells cultured on glass coverslips underwent a rigorous washing with PBS three times. Following this, the cells were fixed in 4 % paraformaldehyde for 15min, and were permeabilized using 0.5 % Triton X-100 solution for 15min at room temperature. After blocking with 10 % normal goat serum for 1h, the cells were incubated with γ-H2AX antibody (ab81299, Abcam) for 1h at room temperature. Subsequently, the cells were washed with PBS three times and incubated with fluorescently labeled Goat Anti-Rabbit secondary antibodies for 1h at room temperature. Cell nuclei were counterstained with DAPI for 5min. The resulting images were captured randomly using a Leica confocal microscope and analyzed with ImageJ software.

2.10. RNA fluorescence in situ hybridization (FISH)

5–8F and CNE-2 cells were used to investigate the colocalization of miR-142-3p with its target proteins. The preliminary procedure resembled those of an IF assay. Cells were fixed with 4 % paraformaldehyde for 15min, and were permeabilized using 0.5 % Triton X-100 solution at room temperature for 15min, and were prehybridized at 37 °C for 20min. Subsequently, hybridization was carried out using FAM-conjugated miR-142-3p probes at 37 °C overnight under dark conditions. Then, the cells were rinsed in 1 × saline-sodium citrate (SSC) buffer at 42 °C. Blocking was performed with PBST containing 5 % bovine serum albumin at room temperature for 30min. Following this, cells were incubated with CFL2 (1:100, 11848-1-AP, Proteintech) or WASL antibody (1:100, 14306-1-AP, Proteintech) for 1h, followed by a reaction with Alexa Fluor 594-conjugated secondary antibodies (1:200, #48934, Cell Signaling Technology) and DAPI (Vector Laboratories) for 30min. Finally, the resulting fluorescent signals were captured using a confocal microscope.

2.11. RNA in situ hybridization (ISH)

The expression levels of miR-142-3p in NPC specimens were detected using a DIG-UTP-labeled miR-142-3p probe (Exonbio, Guangzhou, China). Paraffin-embedded sections underwent a dewaxing process using 100 % ethanol and xylene. Subsequently, the sections with DIG-UTP-labeled probes were incubated at 40 °C for 18h. DAB substrate was used for the colorimetric detection of miR-142-3p. Finally, the sections were co-stained with hematoxylin and dehydrated in xylene and graded alcohols. The staining slides were evaluated and scored according to the staining intensity (negative: 0; weak: 1; medium: 2; and strong: 3) and the abundance of positive cells (≤5 %: 0; 6 %; weak: 1; medium 2; 51%–75 %: 3; and ≥76 %: 4). The final score, calculated by multiplying the intensity score by the abundance score, provided a classification of miR-142-3p expression as either low (0–4) or high (5-12).

2.12. Immunohistochemistry (IHC)

Paraffin-embedded patient samples or mouse tumor tissue samples were sectioned and mounted on slides. These sections were briefy incubated in an oven at 70 °C for 80min, and were subjected to xylene deparafnization twice for 20min and gradient ethanol hydration twice for 5min. For antigen retrieval, the sections were immersed the in a boiling solution of sodium citrate bufer and maintained at a rolling boil for an additional 4min. Then, the slides were treated with a 3 % hydrogen peroxide solution for 15min. The sections were then incubated overnight at 4 °C with primary antibodies against CFL2 (1:200, 11848-1-AP, Proteintech), WASL (1:200, 14306-1-AP, Proteintech), γ-H2AX (1:1000, ab81299, Abcam) and Ki67 (1:2000 , ab15580, Abcam). Afterward, the sections were incubated with biotinylated secondary antibody that was conjugated to a horseradish peroxidase complex. 3,5-diaminobenzidine (DAB) was used to visualize the staining effects and each slide was then meticulously examined and captured blindly using a light microscope. The assessment criteria were identical to those described in the ISH section.

2.13. LC–MS analysis

Pierce Magnetic RNA-Protein Pull-Down Kit (20164, Thermo Fisher) was utilized to enrich potential proteins that bind to pri-miR-142. The biotinylated Sense and Antisense RNA sequences of pri-miR-142 were synthesized as follows. Sense: sequence: GACAGUGCAGUCACCCAUAAAGUAGAAAGCACUACUAACAGCACUGGAGGGUGUAGUGUUUCCUACUUUAUGGAUGAGUGUACUGUG; Antisense sequence: CACAGUACACUCAUCCAUAAAGUAGGAAACACUACACCCUCCAGUGCUGUUAGUAGUGCUUUCUACUUUAUGGGUGACUGCACUGUC.
5–8F cells cultured in a 6-well plate were harvested, and 200 μl Thermo Scientific Pierce IP Lysis Buffer was added. The cells were then lysed on ice for 30min, followed by centrifugation at 10000 rpm at 4 °C for 15min. A 5 μl alipuot of the cell lysate was used for a BCA (Thermo Fisher Scientific, USA) assay. Next, 50 μl streptavidin magnetic beads were added to a 1.5 ml EP tube. The tube was placed in a magnetic rack to collect the beads, and the supernatant was discarded. The beads were resuspended in an equal volume of 20 mM Tris buffer (pH 7.5), and the process of bead collection and supernatant discarding was repeated. Subsequently, an equal volume of 1 × RNA Capture Buffer was added to resuspend the beads, and 50 pmol of biotinylated pri-miR-142 was introduced. The mixture was gently agitated and incubated at room temperature for 30min. After incubation, the EP tube was again palced in the magnetic rack to collect the beads, and the supernatant was discarded. The beads were resuspended in an equal volume of 20 mM Tris (pH 7.5), collected using the magnetic rack, and the supernatant was discarded once more. Then, 100 μl 1 × Protein-RNA Binding Buffer was added, mixed thoroughly, and the beads were collected, discarding the supernatant as before. To prepare the RNA-protein binding reaction mixture, 10 μl of 10 × Protein-RNA Binding Buffer, 30 μl of 50 % glycerol, 30 μl of cell lysate, and 30 μl of water were combined. 100 μl of this mixture was added to the beads, gently mixed, and incubated at 4 °C for 60min. Finally, the EP tube was placed in the magnetic rack to collect

the beads, with the subsequent disposal of the supernatant. The beads were resuspended in 100 μl 1 × wash buffer, and the EP tube was once again placed in the magnetic rack to gather the beads, and the supernatant was discarded. 50 μl Elution Buffer was added to resuspend the beads, followed by incubation at 37 °C for 30min. After incubation, the EP tube was placed back on the magnetic rack, enabling the collection of supernatant containing the final protein samples. These proteins were separated via SDS-PAGE, and strips were manually cut from the gel and digested using sequencing trypsin (Promega, Madison, WI, USA). The digested peptides were analyzed using a Thermo Fisher Q Exactive mass spectrometer (Thermo Fisher, USA). The fragment spectra were analyzed using the UniProt *Homo sapiens* protein database with ProteomeDiscover 2.5.

2.14. Enzyme-linked immunosorbent assay (ELISA)

Treated NPC cell culture supernatants and mouse serum samples were collected and analyzed for cytokines production using ELISA kits according to the manufacturer's instructions. The ELISA kits for CXCL10 (EH6134M, human; EM30138S, mouse), CXCL11 (EM6135M, human; EM30139S, mouse), CCL5 (EH6998M, human; EM30252S, mouse), and IFNβ (EH6241M, human; EM30446S, mouse) were obtained from Biotechwell (Shanghai, China).

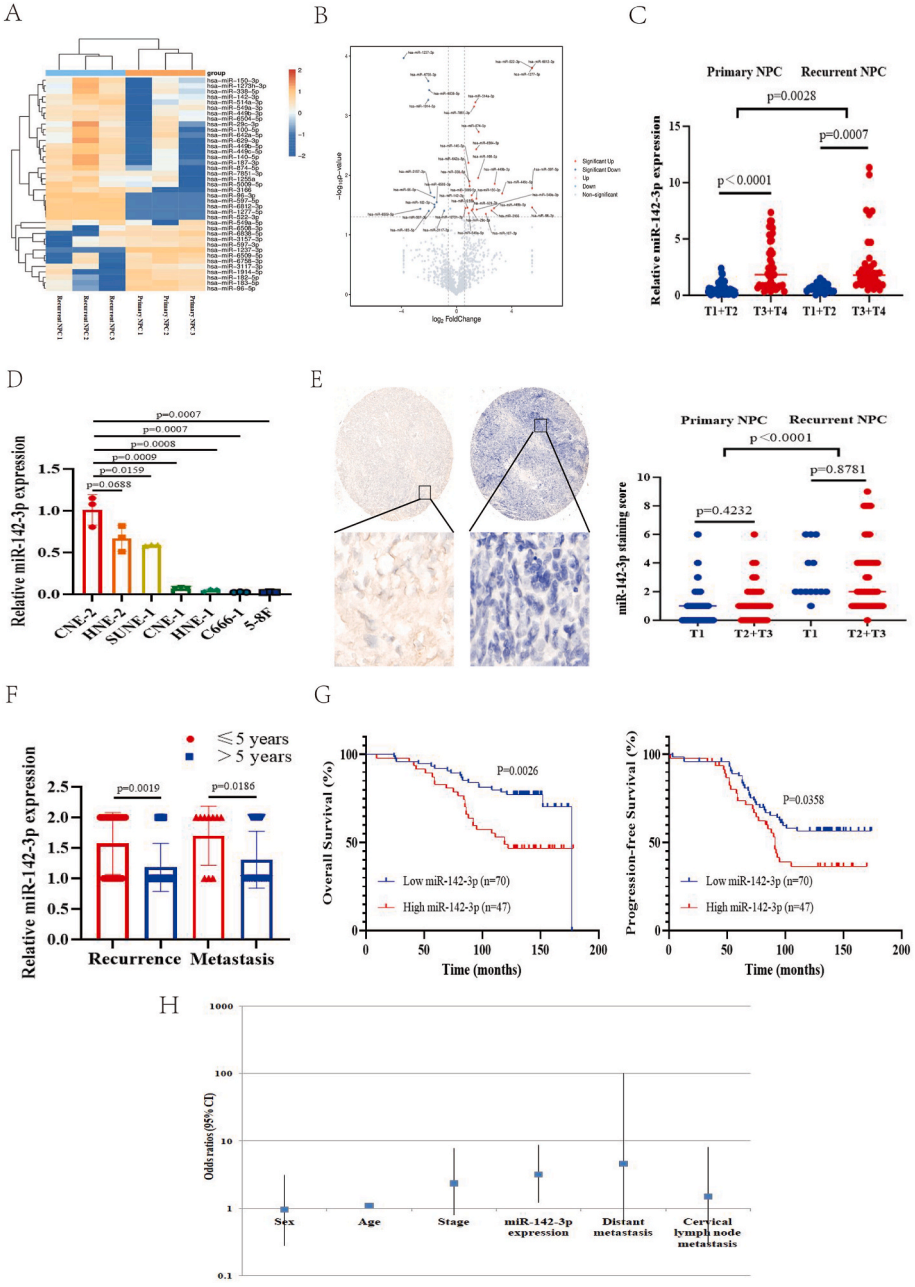

Fig. 1. MiR-142-3p is upregulated and associated with poor prognosis in rNPC. (A) The heatmaps and (B) The volcano plot with hierarchical clustering analysis on the three matched primary versus recurrent NPC tumor tissue pairs shows differentially expressed miRNAs. C RT-PCR analysis of the expression levels of 107 primary NPC tissues and 58 recurrent NPC tissues in different tumor stages. D Relative expression of miR-142-3p in NPC cell lines. U6 was used as an endogenous control. E Localization and expression of miR-142-3p was detected by in situ hybridization in a tissue microarray containing 63 cases of primary NPC and 59 cases of recurrent NPC. F Relationship between miR-142-3p expression and early new tumor events. G Overall survival and progression-free survival of NPC patients with high and low miR-142-3p expression levels. H Multivariate analysis of miR-142-3p expression and multiple clinical parameters.

2.15. Coimmunoprecipitation (Co-IP)

To investigate the potential interaction between ADAR1 and Dicer, 5–8F cells and CNE-2 cells were lysed in 500 μl Co-IP buffer (Thermo Fisher Scientific, USA) supplemented with a cocktail of proteinase, phosphatase, and RNase inhibitors for 30min, followed by centrifugation at 12,000×*g* for 15min. 5 μl of the cell lysate was used for a BCA (Thermo Fisher Scientific, USA) assay. Next, 2 mg of the cell lysate was incubated with 2 μg of the interacting protein antibody (while the control group received 2 μg of an isotype IgG antibody) and 20 μl of protein A/G-beads. The mixture was then agitated on a rotary mixer at 4 °C overnight. The next day, the mixture was placed on a magnetic rack, and the supernatant was discarded. The beads were washed three times with Co-IP buffer. 40 μl of 1 × loading buffer were added to the beads, and this mixture, along with 20 μg of Input, was boiled for 5min. Finally, the retrieved proteins were subjected to Western blot analysis to detect the interaction between ADAR1 and Dicer.

2.16. RNA pull-down assays

For RNA pull-down assay, 1×10^7 cells were washed in ice-cold PBS and lysed in 500 μl of Co-IP buffer (Thermo Scientific, USA) supplemented with a cocktail of proteinase, phosphatase, and RNase inhibitors (Invitrogen, USA). The lysates were incubated with 3 μg of biotinylated DNA oligonucleotide probes targeting the pri-miR-142 backsplice junction region (sense) or its complementary probes (antisense) for 2h at room temperature. Subsequently, 50 μl of washed streptavidin C1 magnetic beads (Invitrogen, USA) were added to each binding reaction and incubated for an additional hour at room temperature. The beads were then washed five times with Co-IP buffer. Finally, the retrieved proteins were used for Western blot analysis. The probe sequences targeting pri-miR-142 was: 5′-CCCTCCGTGCTGTTGTGTGCTTTCTCTT-3’.

2.17. RNA immunoprecipitation (RIP)

RIP experiments were performed with an RNA-Binding Protein Immunoprecipitation Kit (Geneseed, Guangzhou, China) according to the manufacturer’s instructions. 100 μl of lysates from ADAR1-upregulated 5–8F and CNE2 cells (1×10^7) were used as input control. 900 μl of cell lysates were incubated with 5 μg of anti-ADAR1 antibody or IgG-containing protein A/G-agarose beads as a control. After continuous rotation at 4 °C overnight, the beads were washed, and the coprecipitated RNA was measured by RT−PCR. The primer sequences for pri-miR-142 were: Forward (F): 5′-TGCAGTCACCCATAAAGTAGAAAG-3’; Reverse (R): 5′-ACAGTACACTCATCCATAAAGT-3’.

2.18. Electrophoretic mobility shift assay (EMSA)

Pri-miR-142 labeled with FAM at the 5’ terminus (10 nM) was incubated with different dosages of ADAR1 for 40min in a 10 μl reaction solution containing 10 mM HEPES (pH 7.4), 50 mM KCl, 1 mM EDTA, 0.05 % Triton X-100, 5 % glycerol, 0.01 mg/ml BSA and 1 mM DTT. The products were resolved on 1 % agarose gels in 0.5 × Tris-borate-EDTA buffer under an electric field of 15 V/cm for 30min. The gels were subsequently visualized with a Typhoon Trio Imager.

2.19. Luciferase reporter assay

5–8F cells and CNE-2 cells were cotransfected with plasmids containing the 3′-UTR of wild-type or mutant fragments from CFL2 or WASL, along with miR-142-3p mimic, using Lipofectamine 3000 (Invitrogen, CA, USA) according to the manufacturer’s protocol. At 24h post-transfection, the firefly and renilla luciferase activities were consecutively measured using a dual luciferase reporter assay system (Promega, Massachusetts, USA). Finally, the ratios of luminescence from firefly to renilla luciferase were calculated.

2.20. Xenograft tumor experiments

For xenograft experiments, 4- to 6-week-old male nude mice were used. We established three stable overexpression groups in 5–8F cells through lentiviral transduction with vectors encoding miR-142-3p alone, miR-142-3p combined with CFL2, or miR-142-3p with WASL. Conversely, a stable knockdown group was achieved in CNE-2 cells using lentiviral particles encoding miR-142-3p-targeted shRNAs. Subsequently, 5×10^6 treated cells from each group were subcutaneously injected into the dorsal side of the nude mice. Once the tumors became palpable, their size was measured every three days, and the tumor volume was calculated using the modified ellipse formula (volume = length × width^2 × 0.5). After 22–25 days, the mice were sacrificed, and the tumors were dissected. The final tumor weights and volumes were determined after sacrificing the mice.

2.21. Statistical analysis

GraphPad Prism 8 was used for statistical analysis. Data are presented as the mean ± SD from at least three independent experiments. A two-tailed unpaired Student’s *t*-test was used for comparisons between two groups with normal distribution. Kaplan–Meier curves were employed for survival analysis, and statistical significance was determined by the log-rank test. A P-value of less than 0.05 was considered statistically significant. Significance levels are indicated as follows: *P < 0.05, **P < 0.01, ***P < 0.001, ****P < 0.0001.

3. Results

3.1. MiR-142-3p was identified and upregulated in rNPC

To investigate the miRNA expression profile in NPC, we conducted miRNA sequencing analysis of three matched pairs of primary tumor tissues and recurrent tumor tissues. The differentially expressed miRNAs are depicted in Fig. 1A. Notably, miR-142-3p was found significantly upregulated in recurrent NPC compared to primary NPC (Fig. 1B). This finding was further validated through RT-PCR analysis of 107 primary NPC tissues and 58 recurrent NPC tissues (Fig. 1C). Additionally, the expression of miR-142-3p was significantly higher in patients with advanced-stage NPC compared to those with early-stage NPC (Fig. 1C). Upon assessing the expression levels of miR-142-3p in NPC cell lines, we selected 5–8F cells with high expression and CNE-2 cells with low expression for further experiments (Fig. 1D). Next, we analyzed datasets from The Cancer Genome Atlas (TCGA), and discovered that miR-142-3p expression was upregulated in 497 head and neck squamous cell carcinoma tissues compared to 44 normal samples (Fig. S1). To evaluate the clinical significance of miR-142-3p in NPC, we analyzed miR-142-3p expression using in situ hybridization in a tissue microarray containing 63 primary NPC cases and 59 recurrent NPC cases (Table S3). Our findings indicated that recurrent NPC tumor tissues exhibited stronger positive miR-142-3p staining compared to primary NPC tumor tissues (Fig. 1E). Moreover, recurrent NPC patients with early new tumor events, including recurrence ($p = 0.0019$) or metastasis ($p = 0.0186$) within five years post-treatment, exhibited significantly higher miR-142-3p expression levels (Fig. 1F). Survival analyses revealed that high miR-142-3p expression in the NPC tissue microarray was significantly associated with reduced overall survival (OS) and progression-free survival (PFS), but not with metastasis-free survival (Fig. 1G) (Fig. S2). Multivariate analysis showed that miR-142-3p expression was an independent prognostic factor for OS (Fig. 1H). Overall, miR-142-3p is found upregulated in rNPC and is associated with poor prognosis.

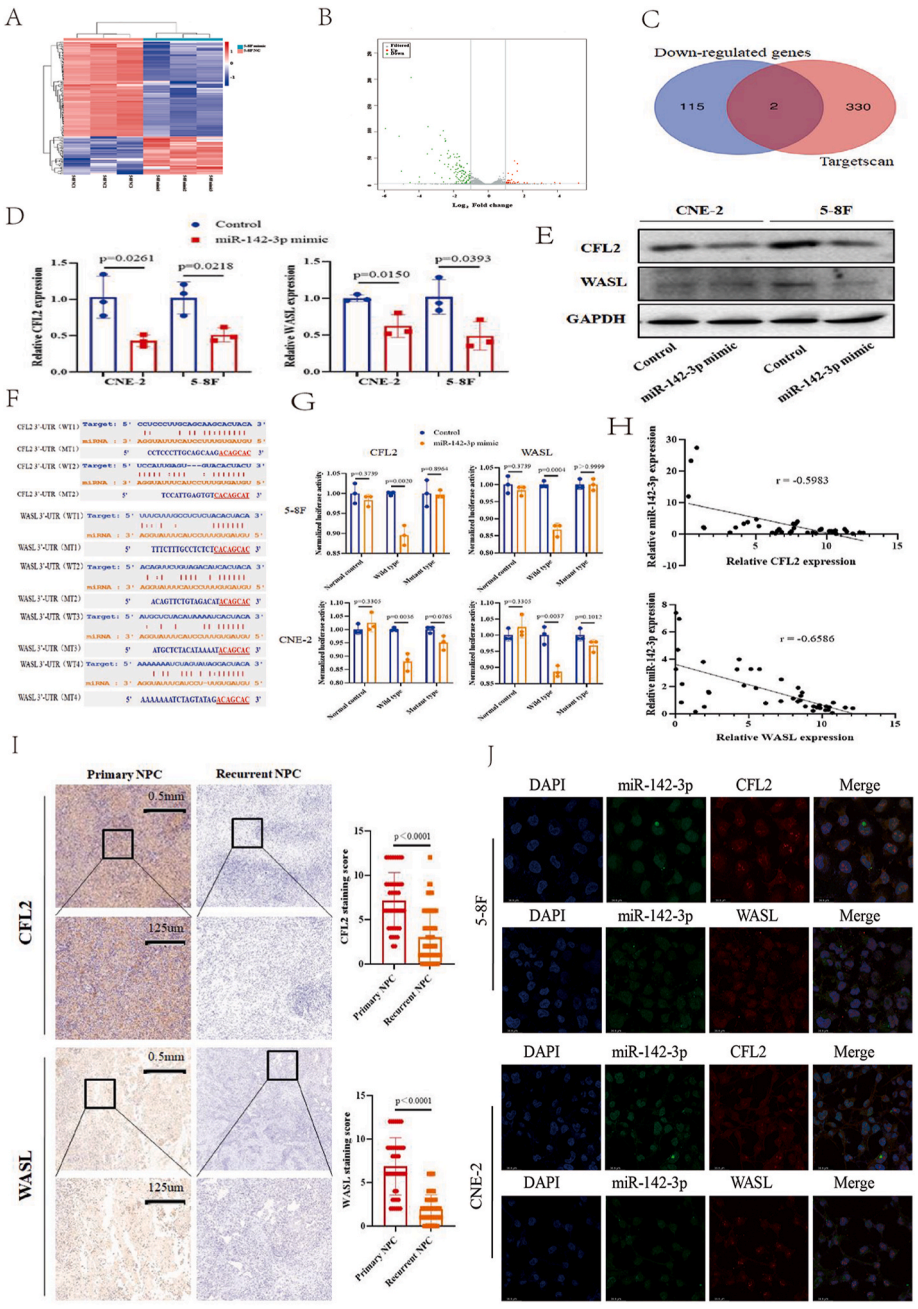

Fig. 2. CFL2 and WASL are direct targets of miR-142-3p. A Transcriptome sequencing of 5–8F cells transfected with miR-142-3p mimic and control mimic. B Differentially downregulated expressed genes detected in the mimic group. C Venn diagram of predicted target genes of miR-142-3p. (D) RT-PCR and (E) Western blotting revealed CFL2 and WASL expression in 5–8F cells and CNE-2 cells transfected with miR-142-3p mimic. F Schematic of the CFL2 and WASL 3′-UTR sequences containing the miR-142-3p binding site and the mutant types of CFL and WASL. G Relative miR-142-3p expression in luciferase activity assay. H Relationship between relative miR-142-3p and CFL2 or WASL in 40 recurrent NPC tissue samples. I Immunohistochemistry assay showing the protein levels of CFL2 and WASL in 43 human primary and 69 recurrent NPC tissues. J Immunofluorescence assays revealed the subcelluar localization of miR-142-3p and CFL2 or WASL in 5–8F and CNE-2 cells.

3.2. CFL2 and WASL are direct targets of miR-142-3p

We next aimed to elucidate the potential targets of miR-142-3p in NPC. To achieve this, we transiently transfected the miR-142-3p mimic and a control mimic into 5–8F cells for transcriptome sequencing (Fig. 2A). According to the criteria of mean fold change >2 and adjusted P value < 0.05, we detected a total of 117 genes that were significantly downregulated in the miR-142-3p mimic group (Fig. 2B). Using prediction programs, the miR-142-3p target genes were predicted. As a result, a total of 332 targets were collected from TargetScan. Then we used TargetScan to identify and validate two candidate targets, CFL2 and WASL (Fig. 2C). Notably, the mRNA and protein expression levels of CFL2 and WASL were significantly reduced in the miR-142-3p mimic group compared to their respective controls (Fig. 2D and E). Fig. 2F illustrates the sequence of predicted miRNA binding sites in the 3′-UTR of CFL2 and WASL. To verify the binding of miR-142-3p to the 3′ end of mCFL2 and mWASL, we cloned the wild type or mutant 3′ miR-142-3p bound to CFL2 and WASL into luciferase reporter plasmids. As expected, the luciferase reporter assay showed that the inhibitory effects of miR-142-3p on CFL2 and WASL were abolished when the predicted

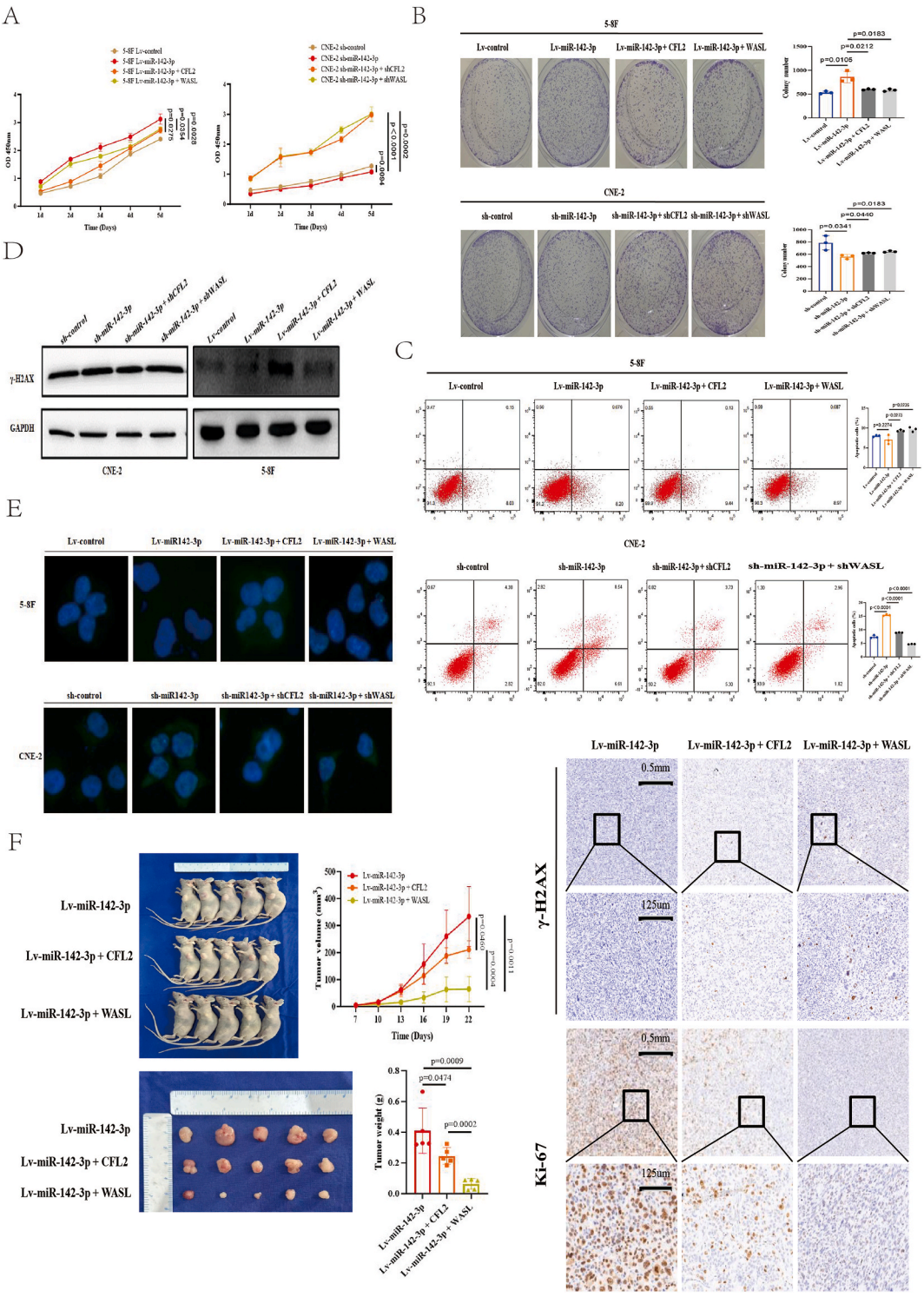

Fig. 3. Overexpressing CFL2 or WASL reverses the NPC progression induced by miR-142-3p. (A) CCK-8 assay, (B) Colony formation assay, (C) Flow cytometry assay, (D) Western blot analysis of γ-H2AX and (E) Immunofluorescence staining of γ-H2AX foci in miR-142-3p-overexpressing cells with or without lentiviral carrying CFL2 or WASL high expression vector and miR-142-3p-knockdown cells with or without lentiviral carrying CFL2 or WASL shRNA. Nuclei were counterstained with DAPI (blue). F 5–8F cells with stable high expression vector of CFL2 and WASL significantly decreased tumorigenicity induced by miR-142-3p in vivo. The growth and weight of subcutaneous xenograft tumors injected with miR-142-3p-overexpressing 5–8F cells with or without CFL2 or WASL high expression vector (n = 5 each group). Immunohistochemistry assay showing the expression of γ-H2AX and Ki67 in miR-142-3p-overexpressing 5–8F cells with or without CFL2 or WASL high expression vector.

binding site of CFL2 and WASL at the 3′-UTR was mutated (Fig. 2G). Additionally, CFL2 and WASL expression was inversely correlated with miR-142-3p expression in recurrent NPC tissue samples as evidenced by RT-PCR analysis (Fig. 2H). Consistent with these findings, IHC analysis of human primary and recurrent NPC tissues revealed a significant reduction in the protein levels of CFL2 and WASL in recurrent NPC tissues compared to primary NPC tissues (Fig. 2I). Additionally, RNA FISH assays confirmed the colocalization of miR-142-3p with CFL2 or WASL

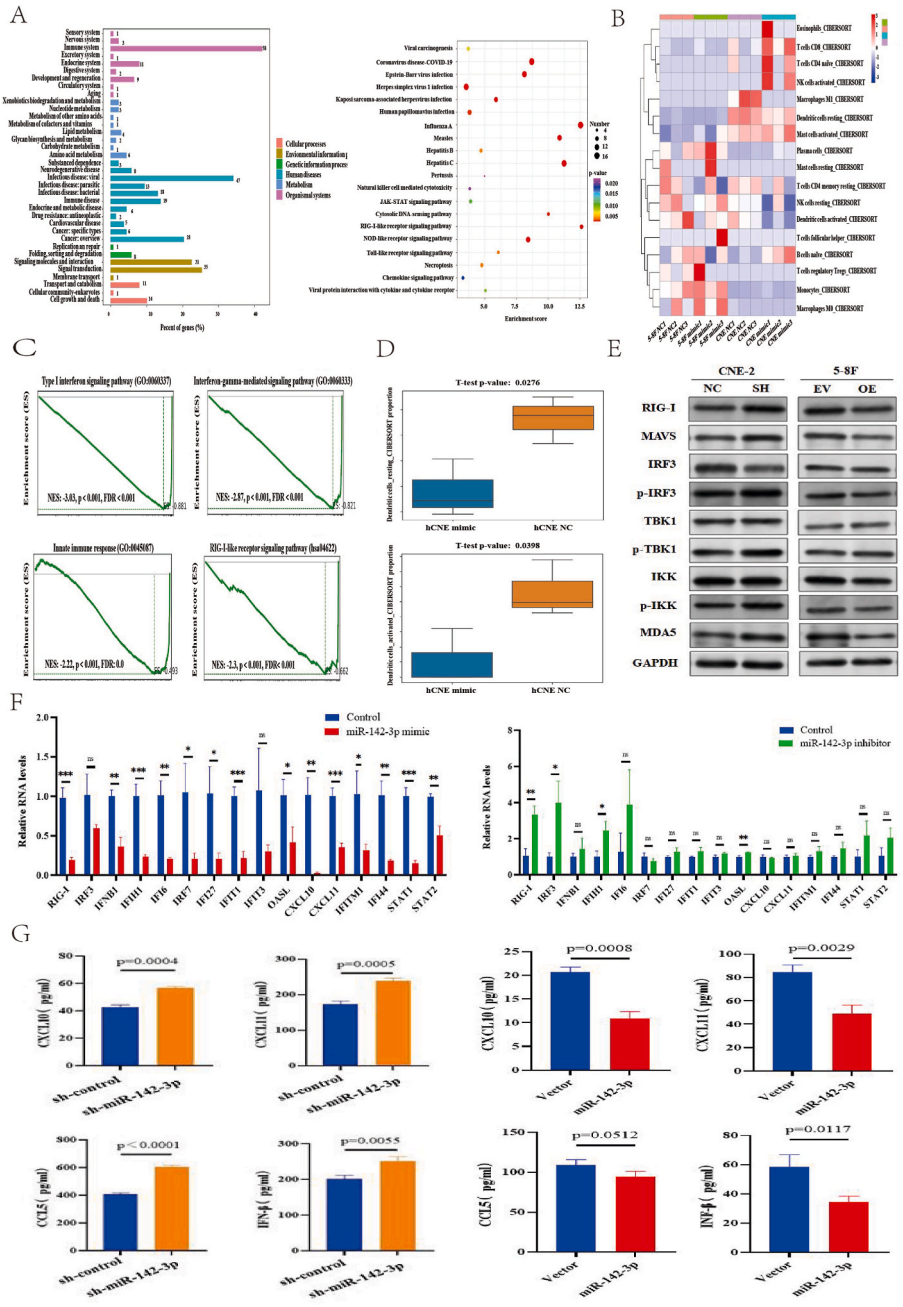

Fig. 4. MiR-142-3p represses the immune defence response and RIG-I signalling pathway in NPC cells. (A) and (B) RNA-sequencing of KEGG pathway enrichment analysis and Gene Ontology biological processes between the miR-142-3p the mimic group and mimic control group. C Gene set enrichment analysis (GSEA) for the miR-142-3p mimic group and mimic control group. DCIBERSORTx analysis of resting and activated dendritic cells between the miR-142-3p mimic group and the mimic control group. E Protein levels in CNE-2 cells with miR-142-3p knockdown and 5–8F cells with miR-142-3p overexpression. F RT-PCR was used to measure the fold change in the indicated mRNAs in CNE-2 cells with miR-142-3p knockdown and 5–8F cells with miR-142-3p overexpression. G ELISA was used to measure the levels of CXCL10, CXCL11, CCL5, and IFN-β in the supernatants of CNE-2 cells with miR-142-3p knockdown and 5–8F cells with miR-142-3p overexpression.

in the cytoplasm of NPC cell lines (Fig. 2J). These results indicate that miR-142-3p directly suppresses CFL2 and WASL expression by binding to their respective 3′-UTR regions in NPC.

3.3. Overexpression of CFL2 or WASL rescues the malignant phenotypes induced by miR-142-3p

To investigate the functions of miR-142-3p and its potential targets in NPC, we introduced lentivirus-mediated overexpression of miR-142-3p, CFL2 and WASL in 5–8F cells, and used antisense oligonucleotides to inhibit miR-142-3p, CFL2 and WASL expression in the CNE-2 cells, which were subsequently validated by RT-PCR (Fig. S3). As expected, upregulation of CFL2 or WASL significantly attenuated miR-142-3p-mediated proliferation (Fig. 3A) and colony-forming ability (Fig. 3B), while concurrently increasing the proportion of apoptotic cells (Fig. 3C). Furthermore, ectopic overexpression of CFL2 or WASL significantly reversed the miR-142-3p-induced downregulation of γ-H2AX expression (Fig. 3D and E). Conversely, silencing CFL2 or WASL expression exerted opposing effects in the aforementioned functional experiments. Moreover, we investigated the potential roles of miR-142-3p and its targets in vivo via a nude mouse xenograft model. Our results demonstrated that CFL2 and WASL overexpression significantly suppressed the

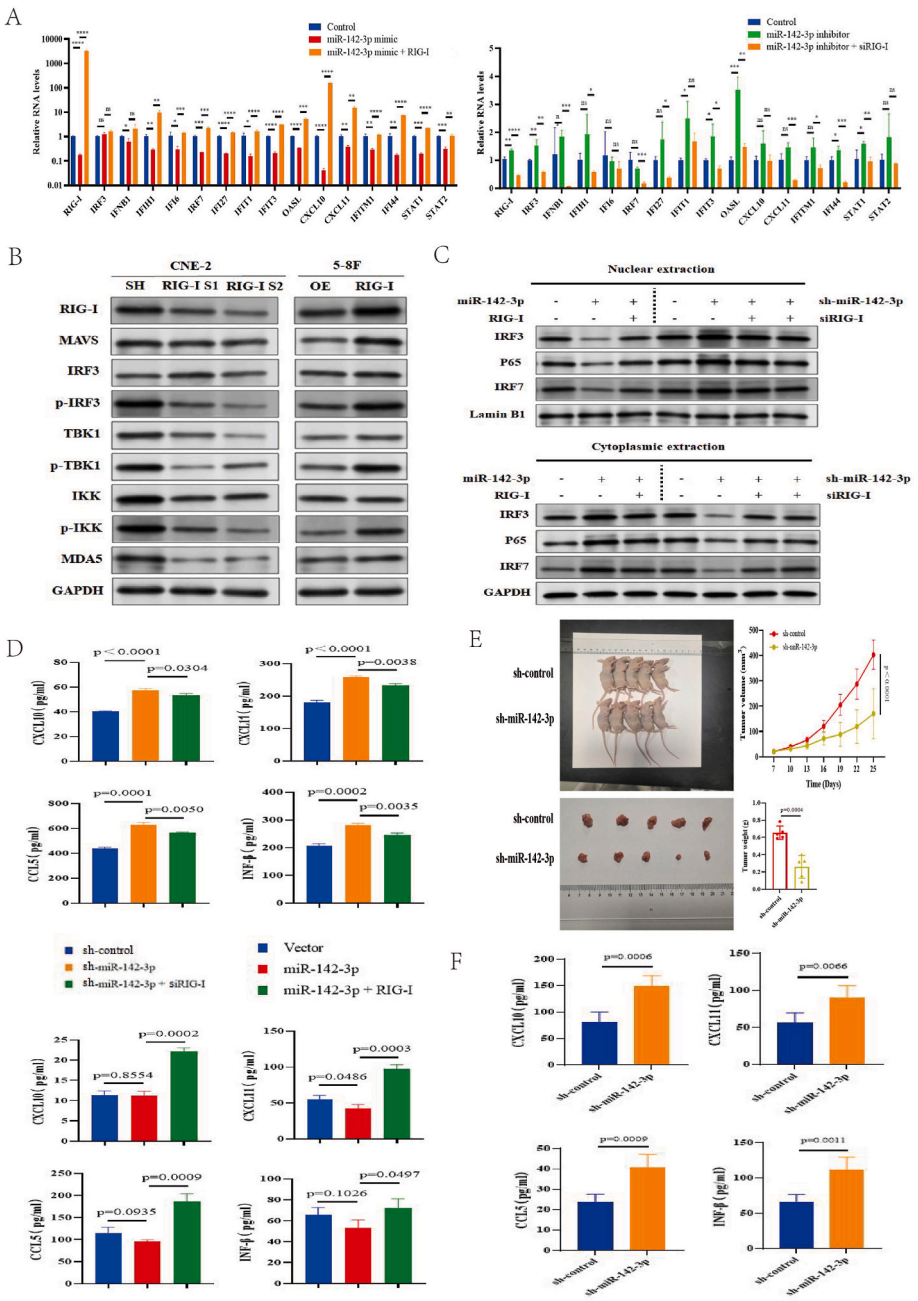

Fig. 5. RIG-I is required for the miR-142-3p-mediated immune response. A Fold change in the indicated mRNAs in miR-142-3p-knockdown cells with or without RIG-I knockdown, and in miR-142-3p-overexpressing cells with or without RIG-I overexpression. B Protein levels in CNE-2 cells with miR-142-3p-knockdown or RIG-I knockdown, and in 5–8F cells with miR-142-3p overexpression or RIG-I overexpression. C Protein levels of IRF3, P65 and IRF7 in the nuclear and cytoplasmic fractions in the indicated cells. D Levels of CXCL10, CXCL11, CCL5, and IFN-β in the supernatants of CNE-2 cells with miR-142-3p knockdown or RIG-I knockdown, and 5–8F cells with miR-142-3p overexpression or RIG-I overexpression. E The volume and weight of subcutaneous xenograft tumors injected with miR-142-3p knockdown CNE-2 cells and control cells (n = 5 mice per group). F Levels of CXCL10, CXCL11, CCL5, and IFN-β in the serum of mice injected with miR-142-3p knockdown CNE-2 cells and control cells (n = 5 mice per group).

tumorigenicity of NPC cells triggered by miR-142-3p overexpression (Fig. 3F). Specifically, tumor tissues overexpressing CFL2 and WASL reversed the miR-142-3p-induced downregulation of γ-H2AX expression and upregulation of Ki67 expression (Fig. 3F). Thus, these results demonstrated that overexpression of CFL2 or WASL can rescue the malignant phenotypes induced by miR-142-3p in NPC.

3.4. MiR-142-3p suppresses the immune defense response and RIG-I signaling pathway in NPC cells

Upon reviewing previous RNA-sequencing results, we observed that miR-142-3p significantly suppressed immune defense and type I interferon (IFN) signaling pathway, as evidenced by KEGG pathway enrichment analysis and Gene Ontology biological processes (GOBP) (Fig. 4A and B). Therefore, we further explored the potential relationship between miR-142-3p and tumor immunity. Consistently, gene set enrichment analysis (GSEA) also revealed a significant involvement of target gene signaling pathways in immune responses, particularly the IFN signaling pathway and the RIG-I-like receptor signaling pathway (Fig. 4C). Addtionally, CIBERSORTx analysis corroborated that NPC tumors exhibiting higher miR-142-3p expression contained fewer infiltrating immune cells, particularly resting and activated dendritic cells

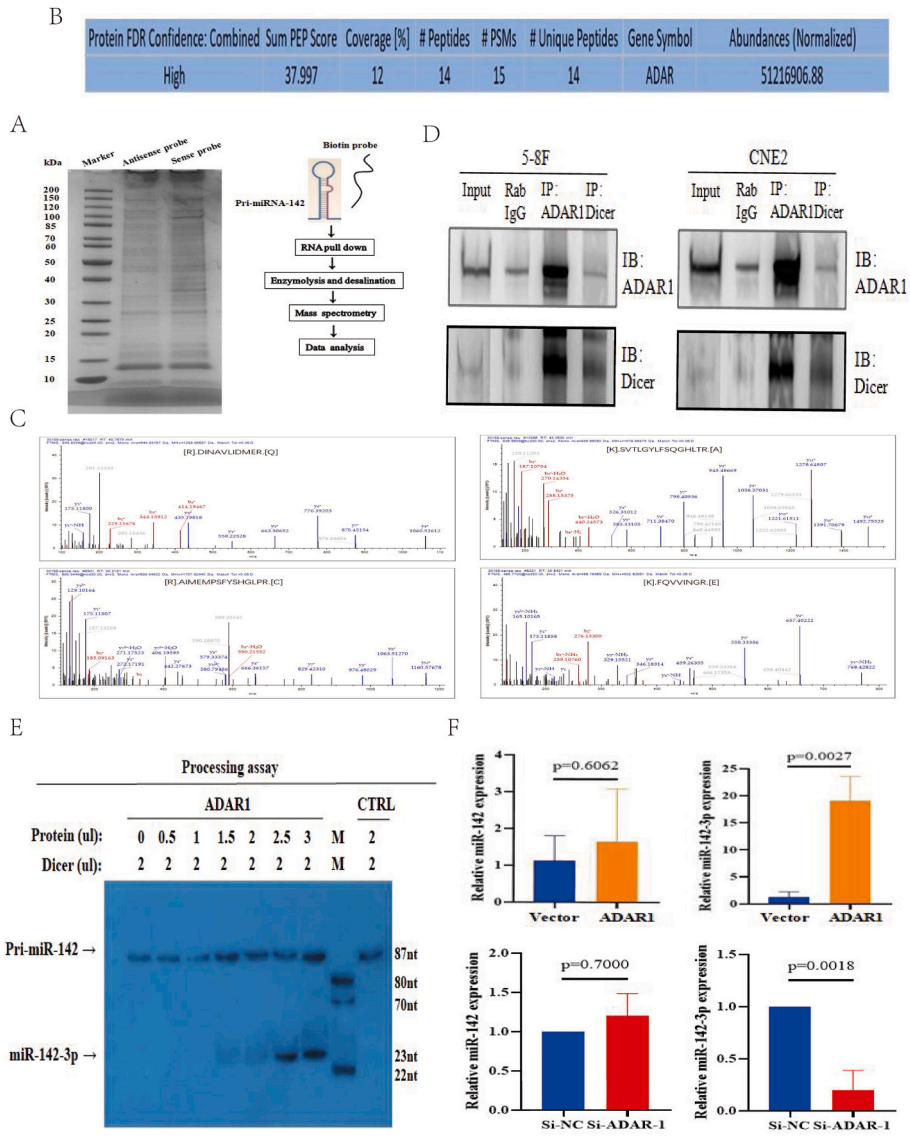

Fig. 6. ADAR1 interacts with and enhances Dicer activity in a dose-dependent manner. A Comparative proteomic study of pri-miR-142 and control. B Detailed information of ADAR1 was presented as potential binding protein with pri-miR-142. C Four representative 2-DE maps of ADAR1. D Co-IP assay of ADAR1 and Dicer in NPC cells. E ADAR1 dose-response analysis of pri-miR-142 cleavage by Dicer in the presence of different concentrations of purified GST-ADAR1 proteins. F Relative expression of miR-142 and miR-142-3p in 5–8F cells transfected with ADAR1 plasmid or CNE-2 cells with siADAR1.

(Fig. 4D), indicating a pivotal role of miR-142-3p in suppressing anti-tumor immunity. Following miR-142-3p overexpression or knockdown, a detailed Western blot analysis of immune genes expression in NPC cells revealed the significant downregulation of RIG-I, MAVS, p-IRF3, IKK, p-IKK, and MDA5 proteins, whereas the levels of IRF3, TBK1, and p-TBK1 remained unaffected (Fig. 4E). Conversely, silencing miR-142-3p significantly upregulated the protein levels of RIG-I, MAVS, p-IRF3, p-TBK1, p-IKK, and MDA5, while IRF3, TBK1, and IKK levels remained largerly unchanged (Fig. 4E). Further, we observed inhibition in the expression of a panel of immune genes in NPC cells with miR-142-3p overexpression (Fig. 4F), whereas miR-142-3p knockdown increased the expression levels of these genes in NPC cells (Fig. 4F). ELISA analysis demonstrated that miR-142-3p knockdown dramatically increased the levels of CXCL10, CXCL11, CCL5, and IFNβ in cell culture supernatants, and miR-142-3p overexpression reduced the levels of these cytokines in cell culture supernatants (Fig. 4G). Collectively, these results demonstrate the inhibitory effect of miR-142-3p on immune responses and the RIG-I signaling pathway in NPC cells.

3.5. RIG-I is required for the miR-142-3p-mediated immune response

Recent studies have demonstrated that exogenous miRNAs potently modulate RIG-I-mediated immune signaling. Our observations indicate that miR-142-3p inhibits RIG-I, prompting us to explore whether RIG-I is essential for miR-142-3p to regulate anti-tumor immunity. In RT-PCR analysis, we discovered that upregulated RIG-I reversed the immune responses inhibited by miR-142-3p overexpression (Fig. 5A), whereas silencing RIG-I abrogated the immune responses activated by the suppression of miR-142-3p (Fig. 5A). To further validate these findings, we examined the expression of immune genes in NPC cells by western blotting following RIG-I overexpression or knockdown. The results showed that the protein levels of RIG-I, MAVS, p-IRF3, TBK1, p-TBK1, IKK, p-IKK and MDA5 in miR-142-3p-silenced NPC cells were significantly downregulated by RIG-I knockdown, while the protein levels of IRF3 remained unaffected (Fig. 5B). Conversely, the protein levels of RIG-I, MAVS, p-IRF3, TBK1, p-TBK1, p-IKK and MDA5 in miR-142-3p-overexpressing NPC cells were significantly upregulated by RIG-I overexpression, while the protein levels of IKK and IRF3 were not affected

(Fig. 5B). Western blot results demonstrated that miR-142-3p suppressed the translocation of IRF3, IRF7 and p65 into the nucleus (Fig. 5C). Similarly, cellular fluorescence assay results showed that miR-142-3p inhibited the nuclear translocation of IRF3, IRF7 and p65, while suppressing miR-142-3p can promote the nuclear translocation of IRF3, IRF7, and p65 (Figs. S4A–C). Furthermore, RIG-I overexpression significantly reversed the downregulation of the protein levels of these genes in nucleus as well as the nuclear translocation of IRF3, IRF7 and p65 induced by miR-142-3p in NPC cells (Fig. 5C). Then, we performed ELISAs to measure the levels of cytokines in NPC cell culture supernatants and found that RIG-I knockdown significantly abrogated the induction of CXCL10, CXCL11, CCL5, and IFNβ concentrations by miR-142-3p knockdown (Fig. 5D). Conversely, RIG-I overexpression reversed the decrease in CXCL10, CXCL11, CCL5, and IFNβ concentration induced by overexpressing miR-142-3p (Fig. 5D). To investigate whether miR-142-3p has the potential to regulate the immune response in vivo, CNE-2 cells with or without miR-142-3p knockdown were delivered into C57BL/6 mice by subcutaneous injection. After a 25-days observation period, we found that miR-142-3p knockdown significantly stimulated the tumorigenicity of CNE-2 cells in vivo (Fig. 5E), and the levels of CXCL10, CXCL11, CCL5, and IFNβ in serum were significantly elevated in the mice injected with miR-142-3p-knockdown CNE-2 cells (Fig. 5F). These results suggest a pivotal role for RIG-I in mediating immune responses of miR-142-3p in NPC.

3.6. ADAR1 interacts with and enhances Dicer activity in a dose-dependent manner

A comparative proteomic analysis of pri-miR-142 and its control counterpart was conducted to identify the proteins involved in miRNA processing (Fig. 6A). After comparing the average 2-DE maps, detailed information on the 547 identified proteins was summarized in Supplementary Table S4. Among these, ADAR1 emerged as a potential interactor with pri-miR-142 (Fig. 6B). Four representative 2-DE maps of ADAR1 were shown in Fig. 6C. As previously reported, pri-miRNAs were cleaved by Dicer to generate the mature miRNAs. Here, we wondered whether ADAR1 promoted miRNA processing by binding to pri-miR-142 and Dicer, and whether ADAR1 exerted an effect on the precursor sequence in an A to I editing manner, thereby affecting the miRNA biogenesis. As expected, a Co-IP experiment was performed to validate the interaction of ADAR1 and Dicer in NPC cells. The results demonstrated that ADAR1 could indeed interact with Dicer (Fig. 6D). This prompted us to hypothesize that ADAR1 might influence Dicer's efficacy in miRNA processing. To test this, we performed in vitro processing of pri-miR-142 in the presence of full-length ADAR1. The addition of the recombinant ADAR1 protein significantly enhanced the cleavage of pri-miR-142 by Dicer compared to the control, and the cleavage level was ADAR1 dose-dependent (Fig. 6E). We further examined whether ADAR1 could promote the maturation of miR-142-3p by RT-PCR and revealed that miR-142-3p was markedly increased in the ADAR1 overexpressing group, while miR-142-3p was significantly reduced in the siADAR1 group. However, pri-miR-142 expression was not significantly changed in the ADAR1 overexpressing or silencing group compared with the respective control groups (Fig. 6F). To investigate the association between ADAR1 and pri-miR-142, we next performed RIP assays and RNA pull down experiments. The results showed that ADAR1 was not bound with pri-miR-142 directly (Fig. S5). These findings implied that ADAR1 could physically interact with Dicer but not with pri-miR-142 and promote the formation of mature miR-142-3p in NPC. Subsequently, we performed comparative miRNA sequencing of 5–8F cells cotransfected with ADAR1 plasmid or a control plasmid to identify the miRNA base mutation sites. However, the results showed that the A to I editing activity of ADAR1 towards pri-miR-142 was not detected in this context (Table S5).

4. Discussion

Tumor progression continues to be a significant obstacle in achieving successful treatment outcomes for primary NPC, often resulting in dismal prognosis for patients. Recent studies have highlighted aberrant miRNAs expression during tumor progression, reflecting disruptions in signaling pathways that govern proliferation, apoptosis, epithelial-to-mesenchymal transition and stemness maintenance [20,21]. Consequently, it is of great significance to identify the key miRNAs regulating the hub genes in the progression of NPC, and explore their potential mechanisms, which can provide a more effective direction for diagnosis or treatment targets in the future. You et al. have revealed that let-7i-5p expression was significantly upregulated in NPC and was associated with advanced stage and recurrence. Let-7i-5p inhibits autophagy and promotes the malignant phenotype of NPC by targeting ATG10 and ATG16L1 [22]. Another finding indicates that PinX1 inhibited the malignant phenotype of NPC cells via p53/miR-200b-regulated EMT, thereby reducing the risk of tumor recurrence [23]. Our study provides novel evidence that expression levels of miR-142-3p are elevated in rNPC tissues compared to primary NPC tissues, and are also associated with inferior OS and PFS in patients with rNPC. A previous study reported that high expression of miR-142-3p in the plasma was correlated with worse prognosis, suggesting its potential as a promising marker for prognosis and therapy monitoring in patients with head and neck cancer [24]. However, Li et al. found that miR-142-3p was significantly downregulated in NPC with distant metastasis using propensity-score-matched miRNA microarray analysis [25]. Bioinformatics analyses have also demonstrated that high miR-142-3p expression is significantly correlated with improved outcomes in NPC [26–28]. These findings highlight the complexity of miRNA roles in NPC progression and the need for further in-depth investigation.

Functionally, miR-142-3p promotes the proliferation and viability of NPC cells in vitro and in vivo. Additionally, overexpression two of its targets, CFL2 and WASL, was able to reverse the malignant phenotypes induced by miR-142-3p. Consistent with this, a study reported by Qi et al. indicated that miR-142-3p accelerated NPC progression through the downregulation of SOCS6 expression [29]. However, in non-small cell lung cancer (NSCLC), the role of miR-142-3p is contrasting, as miR-142-3p overexpression enhanced chemosensitivity by targeting high mobility group box-1 (HMGB1) [30]. Here, miR-142-3p expression was decreased in NSCLC tissues, and its upregulation inhibited NSCLC cell proliferation, migration and invasion [31,32]. Direct targeting and inhibition of CFL2 and WASL by miR-142-3p have also been reported in other disease contexts, such as endometriosis, where it exhibited a strong mechanoregulatory impact on endometrial stroma cells through the downregulation of CFL2 and WASL [33]. Notably, these two potential targets of miR-142-3p have also been identified in models of breast cancer and uveal melanoma [34,35]. We hereby propose that miR-142-3p expression levels exhibit significant variations and exert diverse biological functions across multiple tumor types, even when relying on the same targets.

Endemic nasopharyngeal carcinomas are characterized by high expression of programmed death ligand-1 (PD-L1) and intense infiltration of nonmalignant lymphocytes, making immunotherapy a promising therapeutic option in this context. The search for therapeutic targets to enhance the limited responses to immunotherapy among NPC patients holds significant clinical value. MiRNAs are involved in regulating critical tumor immunity processes, either by targeting specific mRNAs or serving as potential tumor antigens [36]. Multiple studies have underscored the importance of miRNAs in immune regulation and immunotherapy. One study reported that miR-155 overexpression stimulated the infiltration of effector T cells into tumors, thereby increasing PD-L1 expression on cancer cells and enhancing the immunological memory response [37]. Futhermore, a recent novel investigation introduced miR-142-3p as a molecular participant in inflammatory synaptopathy, a new pathogenic hallmark of multiple sclerosis and its mouse model,

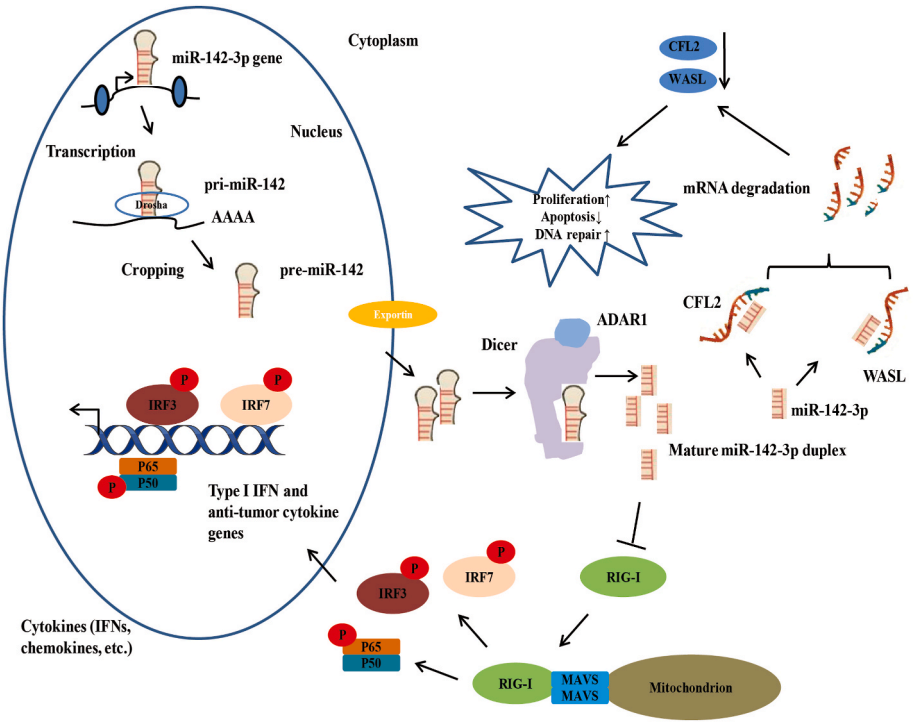

Fig. 7. Outlined functional model for effect of ADAR1-mediated miR-142-3p processing on tumor progression and anti-tumor immunity in NPC.

experimental autoimmune encephalomyelitis, which leads to neuronal loss independent of demyelination [38]. Trobaugh et al. demonstrated that the interaction between the Eastern equine encephalitis virus genome and miR-142-3p limited virus replication in myeloid cells and suppresses the systemic innate immune response [39]. In addition to its involvement in systemic spontaneous immune diseases and antiviral immunity, the role of miR-142-3p in tumor immunity has rarely been reported. Our sequencing results and functional experiments first revealed that miR-142-3p knockdown significantly increased the levels of CXCL10, CXCL11, CCL5, and IFNβ in cell culture supernatants, indicating that miR-142-3p represses the immune defence response and potentially represents a novel target for immunotherapy in NPC.

The activation of the type I IFN signalling pathway is thought to be critical for improving the therapeutic efficacy of ICIs. Our present study found a significant downregulation of RIG-I, MAVS, p-IRF3, IKK, p-IKK, and MDA5 protein levels following the influence of miR-142-3p. Furthermore, we validated the suppression of a panel of immune genes expressions in NPC cells overexpressing miR-142-3p. These results indicated that miR-142-3p could restrain RIG-I-mediated immune responses in NPC. In parallel, Liu et al. have identified several IFNγ-related genes as direct targets of miR-142-3p, noting the hyperactivation of these genes and their signaling pathways in miR-142-deficient Treg cells [40].

Our findings indicated that ADAR1 could physically interact with Dicer, but not with pri-miR-142, to promote the biogenesis of miR-142-3p in a dose-dependent manner. Intriguingly, a previous study demonstrated that ADAR1 may contribute to the progression of oral squamous cell carcinoma by combining with Dicer to regulate oncogenic miRNA maturation and further affect cell migration and invasion[25]. The typical reduction in mature miRNA levels through A to I editing by ADAR1was not observed in current study.

The study has several limitations that merit emphasis. Firstly, a more thorough exploration of how miR-142-3p affects radiation-induced antitumor immunity could yield valuable insights. Secondly, the intricate interaction between ADAR1 and miR-142-3p, and its subsequent facilitation of NPC, requires further elaboration. Finally, additional research is necessary to validate the clinical application potential and prospects of the newly identified targets.

5. Conclusions

Overall, ADAR1-mediated miR-142-3p biogenesis enhances the tumor progression and suppresses antitumor immunity in NPC, indicating that miR-142-3p may serve as potential prognostic biomarkers and therapeutic targets in patients with NPC (Fig. 7).

Funding

This work was financially supported by the National Key Research and Development Program of China (2022YFC2705005), National Natural Science Foundation of China (No. 81870703), Shanghai Shen Kang Hospital Development Center (SHDC12018118), Science and Technology Commission of Shanghai Municipality (20Y11902000, 21ZR1411700, 23YF1404600), and Shanghai Municipal Health Commission (201940143).

CRediT authorship contribution statement

Haoyuan Xu: Writing – original draft. **Wanpeng Li:** Writing – original draft, Funding acquisition. **Kai Xue:** Methodology, Formal analysis. **Huankang Zhang:** Data curation. **Han Li:** Data curation. **Haoran Yu:** Data curation. **Li Hu:** Software, Data curation. **Yurong Gu:** Validation, Supervision. **Houyong Li:** Supervision. **Xicai Sun:** Conceptualization. **Quan Liu:** Funding acquisition, Conceptualization. **Dehui Wang:** Validation, Project administration, Funding acquisition, Conceptualization.

Declaration of competing interest

The authors declare that they have no known competing financialinterestsor personal relationships that could have appeared to influence the work reported in this paper.

Acknowledgments

The authors thank the researchers of the original studies included in this paper.

Appendix A. Supplementary data

Supplementary data to this article can be found online at https://doi.org/10.1016/j.ncrna.2024.08.003.

References

[1] L. Tang, W. Chen, W. Xue, Y. He, R. Zheng, Y. Zeng, W. Jia, Global trends in incidence and mortality of nasopharyngeal carcinoma, Cancer Lett. 374 (1) (2016) 22–30.
[2] K. Wei, R. Zheng, S. Zhang, Z. Liang, Z. Ou, W. Chen, Nasopharyngeal carcinoma incidence and mortality in China in 2010, Chin. J. Cancer 33 (8) (2014) 381–387.
[3] H. Sung, J. Ferlay, R. Siegel, M. Laversanne, I. Soerjomataram, A. Jemal, F. Bray, Global cancer statistics 2020: GLOBOCAN estimates of incidence and mortality worldwide for 36 cancers in 185 countries, CA Cancer J Chin 71 (3) (2021) 209–249.
[4] X. Ding, W. Zhang, R. You, X. Zou, Z. Wang, Y. Ouyang, L. Peng, Y. Liu, C. Duan, Q. Yang, et al., Camrelizumab plus apatinib in patients with recurrent or metastatic nasopharyngeal carcinoma: an open-label, single-arm, phase II study, J. Clin. Oncol. 41 (14) (2023) 2571–2582.
[5] S. Tastsoglou, A. Alexiou, D. Karagkouni, G. Skoufos, E. Zacharopoulou, A. Hatzigeorgiou, DIANA-microT 2023: including predicted targets of virally encoded miRNAs, Nucleic Acids Res. 51 (2023) W148–W153.
[6] H. Huang, Y. Lin, S. Cui, Y. Huang, Y. Tang, J. Xu, J. Bao, Y. Li, J. Wen, H. Zuo, et al., miRTarBase update 2022: an informative resource for experimentally validated miRNA-target interactions, Nucleic Acids Res. 50 (2022) D222–D230.
[7] S. Zou, S. Chen, G. Rao, G. Zhang, M. Ma, B. Peng, X. Du, W. Huang, W. Lin, Y. Tian, et al., Extrachromosomal circular MiR-17-92 amplicon promotes hepatocellular carcinoma, Hepatology 79 (1) (2024) 79–95.
[8] J. Hu, W. Liu, X. Zhang, G. Shi, X. Yang, K. Zhou, B. Hu, F. Chen, C. Zhou, W. Lau, et al., Synthetic miR-26a mimics delivered by tumor exosomes repress hepatocellular carcinoma through downregulating lymphoid enhancer factor 1, Hepatol Int 17 (5) (2023) 1265–1278.
[9] L. Song, J. Yang, Z. Qin, C. Ou, R. Luo, W. Yang, L. Wang, N. Wang, S. Ma, Q. Wu, et al., Multi-targeted and on-demand non-coding RNA regulation nanoplatform against metastasis and recurrence of triple-negative breast cancer, Small 19 (23) (2023) e2207576.
[10] J. Wang, J. Ge, Y. Wang, F. Xiong, J. Guo, X. Jiang, L. Zhang, X. Deng, Z. Gong, S. Zhang, et al., EBV miRNAs BART11 and BART17-3p promote immune escape through the enhancer-mediated transcription of PD-L1, Nat. Commun. 13 (1) (2022) 866.
[11] X. Zhou, Y. Lin, Y. Chen, L. Wang, X. Peng, J. Liao, H. Zeng, W. Luo, D. Wu, L. Cai, Epstein-Barr virus (EBV) encoded microRNA BART8-3p drives radioresistance-associated metastasis in nasopharyngeal carcinoma, J. Cell. Physiol. 236 (9) (2021) 6457–6471.
[12] Y. Hu, T. Setayesh, F. Vaziri, X. Wu, S. Hwang, X. Chen, W. Yvonne, miR-22 gene therapy treats HCC by promoting anti-tumor immunity and enhancing metabolism, Mol. Ther. 31 (6) (2023) 1829–1845.
[13] I. Wang, E. So, J. Devlin, Y. Zhao, M. Wu, V. Cheung, ADAR regulates RNA editing, transcript stability, and gene expression, Cell Rep. 5 (3) (2013) 849–860.
[14] H. Ota, M. Sakurai, R. Gupta, L. Valente, B. Wulff, K. Ariyoshi, H. Iizasa, R. Davuluri, K. Nishikura, ADAR1 forms a complex with Dicer to promote microRNA processing and RNA-induced gene silencing, Cell 153 (3) (2013) 575–589.
[15] M. Tan, Q. Li, R. Shanmugam, R. Piskol, J. Kohler, A. Young, K. Liu, R. Zhang, G. Ramaswami, K. Ariyoshi, et al., Dynamic landscape and regulation of RNA editing in mammals, Nature 550 (7675) (2017) 249–254.
[16] Y. Nemlich, E. Baruch, M. Besser, E. Shoshan, M. Bar-Eli, L. Anafi, I. Barshack, J. Schachter, R. Ortenberg, G. Markel, ADAR1-mediated regulation of melanoma invasion, Nat. Commun. 9 (1) (2018) 2154.
[17] K. Nishikura, M. Sakurai, K. Ariyoshi, H. Ota, Antagonistic and stimulative roles of ADAR1 in RNA silencing, RNA Biol. 10 (8) (2013) 1240–1247.
[18] K. Nishikura, A-to-I editing of coding and non-coding RNAs by ADARs, Nat. Rev. Mol. Cell Biol. 17 (2) (2016) 83–96.
[19] L. Keegan, A. Leroy, D. Sproul, M. O'Connell, Adenosine deaminases acting on RNA (ADARs): RNA-editing enzymes, Genome Biol. 5 (2) (2004) 209.
[20] M. Naldini, G. Casirati, M. Barcella, P. Rancoita, A. Cosentino, C. Caserta, F. Pavesi, E. Zonari, G. Desantis, D. Gilioli, et al., Longitudinal single-cell profiling of chemotherapy response in acute myeloid leukemia, Nat. Commun. 14 (1) (2023) 1285.
[21] E. Kashani, D. Schnidrig, A. Gheinani, M. Ninck, P. Zens, T. Maragkou, U. Baumgartner, P. Schucht, G. Rätsch, M. Rubin, et al., Integrated longitudinal analysis of adult grade 4 diffuse gliomas with long-term relapse interval revealed upregulation of TGF-β signaling in recurrent tumors, Neuro Oncol. 25 (4) (2023) 662–673.
[22] B. You, P. Zhang, M. Gu, H. Yin, Y. Fan, H. Yao, S. Pan, H. Xie, T. Cheng, H. Liu, et al., Let-7i-5p promotes a malignant phenotype in nasopharyngeal carcinoma via inhibiting tumor-suppressive autophagy, Cancer Lett. 531 (2022) 14–26.
[23] C. Yu, F. Chen, X. Wang, Z. Cai, M. Yang, Q. Zhong, J. Feng, J. Li, C. Shen, Z. Wen, Pin2 telomeric repeat factor 1-interacting telomerase inhibitor 1 (PinX1) inhibits nasopharyngeal cancer cell stemness: implication for cancer progression and therapeutic targeting, J. Exp. Clin. Cancer Res. 39 (1) (2020) 31.
[24] I. Summerer, K. Unger, H. Braselmann, L. Schuettrumpf, C. Maihoefer, P. Baumeister, T. Kirchner, M. Niyazi, E. Sage, H. Specht, et al., Circulating microRNAs as prognostic therapy biomarkers in head and neck cancer patients, Br. J. Cancer 113 (1) (2015) 76–82.
[25] X. Liu, Y. Fu, J. Huang, M. Wu, Z. Zhang, R. Xu, P. Zhang, S. Zhao, L. Liu, H. Jiang, ADAR1 promotes the epithelial-to-mesenchymal transition and stem-like cell phenotype of oral cancer by facilitating oncogenic microRNA maturation, J. Exp. Clin. Cancer Res. 38 (1) (2019) 315.
[26] X. Zhang, X. Li, C. Wang, S. Wang, Y. Zhuang, B. Liu, X. Lian, Identification of markers for predicting prognosis and endocrine metabolism in nasopharyngeal carcinoma by miRNA-mRNA network mining and machine learning, Front. Endocrinol. 14 (2023) 1174911.
[27] Z. Zou, S. Liu, Y. Ha, B. Huang, Construction and analysis of lncRNA-mediated ceRNA network in nasopharyngeal carcinoma based on weighted correlation network analysis, BioMed Res. Int. 2020 (2020) 1468980.
[28] S. Zhang, W. Yue, Y. Xie, L. Liu, S. Li, W. Dang, S. Xin, L. Yang, X. Zhai, P. Cao, et al., The four-microRNA signature identified by bioinformatics analysis predicts the prognosis of nasopharyngeal carcinoma patients, Oncol. Rep. 42 (5) (2019) 1767–1780.
[29] X. Qi, J. Li, C. Zhou, C. Lv, M. Tian, MiR-142-3p suppresses SOCS6 expression and promotes cell proliferation in nasopharyngeal carcinoma, Cell. Physiol. Biochem. 36 (5) (2015) 1743–1752.
[30] Y. Chen, X. Zhou, J. Qiao, A. Bao, MiR-142-3p overexpression increases chemo-sensitivity of NSCLC by inhibiting HMGB1-mediated autophagy, Cell. Physiol. Biochem. 41 (4) (2017) 1370–1382.
[31] J. Liu, W. Tian, W. Zhang, Y. Jia, X. Yang, Y. Wang, J. Zhang, MicroRNA-142-3p/MALAT1 inhibits lung cancer progression through repressing β-catenin expression, Biomed. Pharmacother. 114 (2019) 108847.
[32] C. Jin, L. Xiao, Z. Zhou, Y. Zhu, G. Tian, S. Ren, MiR-142-3p suppresses the proliferation, migration and invasion through inhibition of NR2F6 in lung adenocarcinoma, Hum. Cell 32 (4) (2019) 437–446.
[33] C. Börschel, A. Stejskalova, S. Schäfer, L. Kiesel, M. Götte, miR-142-3p reduces the size, migration, and contractility of endometrial and endometriotic stromal cells by targeting integrin- and rho GTPase-related pathways that regulate cytoskeletal function, Biomedicines 8 (8) (2020).
[34] A. Schwickert, E. Weghake, K. Brüggemann, A. Engbers, B. Brinkmann, B. Kemper, J. Seggewiß, C. Stock, K. Ebnet, L. Kiesel, et al., microRNA miR-142-3p inhibits breast cancer cell invasiveness by synchronous targeting of WASL, integrin alpha V, and additional cytoskeletal elements, PLoS One 10 (12) (2015) e0143993.
[35] D. Peng, J. Dong, Y. Zhao, X. Peng, J. Tang, X. Chen, L. Wang, D. Hu, P. Reinach, J. Qu, et al., miR-142-3p suppresses uveal melanoma by targeting CDC25C, TGFβR1, GNAQ, WASL, and RAC1, Cancer Manag. Res. 11 (2019) 4729–4742.
[36] Q. Zhang, W. Wang, Q. Zhou, C. Chen, W. Yuan, J. Liu, X. Li, Z. Sun, Roles of circRNAs in the tumour microenvironment, Mol. Cancer 19 (1) (2020) 14.
[37] S. Sharma, M. Opyrchal, X. Lu, Harnessing tumorous flaws for immune supremacy: is miRNA-155 the weak link in breast cancer progression? J. Clin. Invest. 132 (19) (2022).
[38] F. De Vito, A. Musella, D. Fresegna, F. Rizzo, A. Gentile, M. Stampanoni Bassi, L. Gilio, F. Buttari, C. Procaccini, A. Colamatteo, et al., MiR-142-3p regulates synaptopathy-driven disease progression in multiple sclerosis, Neuropathol. Appl. Neurobiol. 48 (2) (2022) e12765.
[39] D. Trobaugh, C. Sun, N. Bhalla, C. Gardner, M. Dunn, W. Klimstra, Cooperativity between the 3' untranslated region microRNA binding sites is critical for the virulence of eastern equine encephalitis virus, PLoS Pathog. 15 (10) (2019) e1007867.
[40] G. Liu, W. Li, D. Wang, H. Liang, X. Lv, Y. Ye, C. Zhao, L. Ke, S. Lv, N. Lu, et al., Effect of capecitabine maintenance therapy plus best supportive care vs best supportive care alone on progression-free survival among patients with newly diagnosed metastatic nasopharyngeal carcinoma who had received induction chemotherapy: a phase 3 randomized clinical trial, JAMA Oncol. 8 (4) (2022) 553–561.